

# Anisotropic superconducting properties of aligned $\text{MgB}_2$ crystallites

O. F. de Lima, R. A. Ribeiro, M. A. Avila, C. A. Cardoso and A. A. Coelho

*Instituto de Física "Gleb Wataghin", UNICAMP, 13083-970, Campinas, SP, Brazil.*

(Mar 13, 2001)

Samples of aligned  $\text{MgB}_2$  crystallites have been prepared, allowing the identification of an upper critical field anisotropy  $H_{c2}^{ab}/H_{c2}^c \simeq 1.7$ . This implies an anisotropy of the coherence length  $\xi_{ab}/\xi_c \simeq 1.3$  with  $\xi_{o,ab} \simeq 70$  Å,  $\xi_{o,c} \simeq 54$  Å, and a mass anisotropy ratio  $m_{ab}/m_c \simeq 0.6$ . A significant influence of Fe contamination was identified, possibly related to the purity of the raw materials.

The recent discovery of superconductivity at 39 K in Magnesium Diboride ( $\text{MgB}_2$ )<sup>1</sup> has brought new excitement to the area of basic and applied research on superconducting materials. The observation of an isotope effect<sup>2</sup>, a BCS-type energy gap measured by Scanning Tunneling Spectroscopy<sup>3</sup>, as well as band structure studies<sup>4,5</sup>, point to a phonon-mediated superconductivity in  $\text{MgB}_2$ . Some reports<sup>6,7</sup> have suggested that  $\text{MgB}_2$  has an isotropic (or 3D) behavior, based on measurements done in polycrystalline samples. However, other studies<sup>8</sup> have also discussed its possible anisotropic nature. The relatively high values reported for the critical current density<sup>6,9</sup> ( $J_c$ ) are possibly indicating the absence of weak link problems, which are well known in the high- $T_c$  materials. While polycrystalline  $\text{MgB}_2$  is very easy to grow and is a readily available reagent, good-sized single crystals of this material have not yet been reported, and their development promises to be a greater challenge. Here we present results from samples of aligned  $\text{MgB}_2$  crystallites that establish the anisotropy of the upper critical field ( $H_{c2}$ ), thus implying an anisotropic character for all superconducting properties, e.g., the energy gap, coherence length ( $\xi$ ), field penetration depth ( $\lambda$ ), and  $J_c$ .

In this work, a weakly sintered sample of  $\text{MgB}_2$  was prepared, starting with a stoichiometric mixture of 99.5 at% pure Boron and 99.8 at% pure Manganese, both in chips form (Johnson Matthey Electronics). The loose mixture was sealed in a Ta tube under Ar atmosphere, which was then encapsulated in a quartz ampoule and put into the furnace. The compound formation was processed by initially holding the furnace temperature at 1200°C for 1 hour, followed by a decrease to 700°C (10°C/h), then to 600°C (2°C/h), and finally to room temperature at a rate of 100°C/h. The weakly sintered product was easily crushed and milled employing mortar and pestle. Using a stereomicroscope we could observe a very uniform powder consisting mainly of shiny crystallites, with aspect ratios ranging from 2 to 5. This is mainly due to the main surface size distribution ranging from 5 to 40  $\mu\text{m}$  for the larger linear dimension, since the crystallites' thickness is very regular, around 2  $\mu\text{m}$ . The powder was then sieved into a range of particle sizes between 5 - 20  $\mu\text{m}$ , which allows the crystallites fraction to be maximized to almost 100%. Small amounts of the powder were then patiently spread on both sides of a

small piece of paper, producing an almost perfect alignment of the crystallites, as shown in the SEM picture in the upper part of Fig. 1. The lower part of this figure shows an X-ray diffraction pattern from a sample of the *crystallite-painted* paper, displaying only the (001) and (002) reflections coming from the  $\text{MgB}_2$  phase. A lattice parameter  $c = 3.518 \pm 0.008$  Å was evaluated from these two peak positions. The two small impurity peaks marked with asterisks were indexed as  $\text{SiO}_2$ .

Electron microprobe analysis done on four different areas between the  $\text{MgB}_2$  crystallites, revealed the following average concentration (in at%) of elements: O (62.9), C (22.2), Ca (9.48), Si (1.48), Mg (1.44), Al (1.37), K (0.09), Fe (0.50), Cr (0.21), Ni (0.09). The first eight elements in this list were found also in the composition analysis made on the same type of paper used (Canson, ref. 4567-114). The average composition found on top of several crystallites was: Mg (92.50), O (6.70), Ca (0.52), Si (0.21), Fe (0.18). Boron is too light an element and does not show-up in the microprobe analysis. The contaminants found on the crystallites could well be originated from the raw materials, or from the surface contamination caused by the alignment technique, that required vigorous rubbing on top of the powder, using a steel tweezers tip to spread the crystallites uniformly. On the other hand, the inter-crystallite type of *rubbish* is attributed mainly to the paper abrasion, which produces a varied distribution of irregular grains of paper fragments. In order to characterize the superconducting and magnetic properties of the aligned crystallites, we mounted several samples consisting of a pile of 5 small squares ( $3 \times 3$  mm<sup>2</sup>) cut from the painted paper and glued with Araldite resin. Each one of these samples contains a number of crystallites estimated to be around  $6.5 \times 10^5$ , totalizing an effective volume of 0.065 mm<sup>3</sup>.

Figure 2 shows the anisotropic signature of the  $H_{c2}(T)$  line in the field interval  $0 \leq H \leq 40$  kOe. The values were taken from the transition onset of the real component ( $\chi'$ ) of ac susceptibility, measured using a PPMS-9T machine (Quantum Design), with an excitation field of amplitude 1 Oe and frequency 5 kHz. The inset shows an enlarged view of the  $\chi'(T)$  curves for H parallel (solid symbols) and perpendicular (open symbols) to the sample c axis. The  $\chi'(T)$  as well as the  $M(T)$  (inset of Fig. 3) measurements, for  $H = 10$  Oe, show sharp tran-

sitions at the same critical temperature  $T_c = 39.2$  K. Typically, some of the published data on the temperature dependence<sup>2,9-11</sup> of  $H_{c2}(T)$  agree with our result for  $H_{c2}(T) // ab$ . As an example, the data from Ref. 11 is plotted in Fig. 2 as stars. This could simply mean that in polycrystalline samples the transitions are broadened, showing the onset at the highest temperature that corresponds to the highest critical field available, which is  $H_{c2}(T) // ab$ .

The ratio  $\eta = H_{c2}^{ab}/H_{c2}^c$ , between the upper critical field when  $H$  is applied parallel to the  $ab$  plane, and when it is along the  $c$  direction, was evaluated at different temperatures, producing  $\eta = 1.73 \pm 0.03$ . Using the Ginzburg-Landau mean field expression<sup>12</sup> (in CGS units)  $\xi(T) = \xi_o (1 - T/T_c)^{-1/2}$  and that  $H_{c2}^c(T) = \phi_o/(2\pi \xi_{ab}^2)$ , where  $\phi_o = 2.07 \times 10^{-7}$  G cm<sup>2</sup> is the quantum of flux, we find that  $\xi_{o,ab}/\xi_{o,c} = \xi_{ab}(T)/\xi_c(T) = \eta^{1/2} \simeq 1.3$ . Since at  $T = 27$  K we have  $H_{c2}^c = 20$  kOe, this implies that  $\xi_{o,ab} \simeq 70$  Å and  $\xi_{o,c} \simeq 54$  Å, leading to a mass anisotropy ratio<sup>13</sup>  $\varepsilon^2 = m_{ab}/m_c = (\xi_c/\xi_{ab})^2 \simeq 0.6$ . This value is close to 1, which is much larger than  $\varepsilon^2 \simeq 0.04$  or  $10^{-4}$ , respectively for the YBCO and BSCCO high-Tc cuprates, known to be highly anisotropic materials<sup>13</sup>.

The magnetization curves  $M(T)$  and  $M(H)$ , displayed in Figs. 3 and 4, were measured using a SQUID magnetometer (Quantum Design, model MPMS-5). The  $M(H)$  curves ( $T = 5$  K) shown in Fig. 3 are very intriguing in the region  $-1 \lesssim H \lesssim 1$  kOe, where the maximum shielding and first field penetration (in the initial virgin state) occur. For  $|H| \gtrsim 1$  kOe the hysteretical curves in both field directions look very similar. However, for  $|H| \gtrsim 40$  kOe (not shown here) the magnetization difference between the up and down curves ( $\Delta M$ ) becomes smaller than the noise. Large fluctuations of the magnetic moment were consistently observed in this field region, for 3 different aligned samples and temperatures ( $T = 5, 10, 20$  K). We suspect that all these observed anomalies are associated with the relatively high ferromagnetic background caused by the presence of almost 2000 ppm of Fe detected in the crystallites. We also suspect that this could be a general problem in most of the published data so far, associated with the raw materials degree of purity. Besides the fast drop of  $J_c$  at higher fields<sup>9,10,14</sup> it has also been very intriguing that most of the reported  $M(T)$  curves for  $H = 10$  Oe display a steady paramagnetic increase, starting at the lowest temperature ( $T \approx 5$  K), even for the ZFC protocol (see inset Fig. 3). We propose that Fe may be acting as a *pair-breaking* agent, thus requiring a careful analysis to separate this effect correctly. Fig. 4 shows an unequivocal signature of the ferromagnetic hysteresis loop measured at  $T = 45$  K (nearly the same result was obtained at  $T = 55$  K). The inset displays an enlarged view close to  $H = 0$  indicating that demagnetization effects are also observed for the  $H // ab$  and  $H // c$  orientations. In a recent detailed study<sup>8</sup> the relevance of Fe contamination has already been identified, through measurements of MgB<sub>2</sub> samples made from commercial powder supplied by a different company.

In view of the contamination problem described above, we have found that it is not reliable to discuss the expected anisotropy in  $J_c \propto \Delta M$ , which could be determined using the Bean model<sup>15</sup>. A rough estimate for both field orientations gives  $J_c \simeq 10^6$  A/cm<sup>2</sup> at  $H = 1.5$  kOe and  $T = 5$  K (Fig. 3). This calculation neglects the small influence of the ferromagnetic hysteresis and considers the average crystallite geometry as described before. However, an anisotropy between  $J_c(H//c)$  and  $J_c(H//ab)$  should be expected. Indeed, independently of the different regime of vortex pinning,  $J_c$  is predicted<sup>13</sup> to be proportional to  $\xi^2$ , leading to  $J_c(H//c) / J_c(H//ab) \approx (\xi_{ab}/\xi_c)^2 \approx H_{c2}^{ab}/H_{c2}^c$ .

A final cautionary observation has to be addressed to the possibility that surface superconductivity could also be occurring for  $H//ab$ , since coincidentally the surface nucleation field is<sup>16</sup>  $H_{c3} \simeq 1.7 H_{c2}$ . However, we have made several careful measurements of  $M(H)$  and  $\chi'(H)$ , as well as  $M(T)$  and  $\chi'(T)$ , around the onset of transition, and no signature<sup>17</sup> of a surface nucleation field was found.

In conclusion, we have prepared samples of aligned MgB<sub>2</sub> crystallites that allowed the identification of anisotropy for the upper critical field given by  $H_{c2}^{ab}/H_{c2}^c \simeq 1.7$ , implying an anisotropy of the coherence length  $\xi_{ab}/\xi_c \simeq 1.3$  and a mass anisotropy ratio  $m_{ab}/m_c \simeq 0.6$ . This could be considered a small anisotropy when compared to the values found for the high-Tc materials ( $m_{ab}/m_c \lesssim 0.04$ ). The problem with Fe contamination has to be solved in order to get more complete and reliable characterization of the intrinsic superconducting parameters. Naturally the production of a good-sized single crystal of MgB<sub>2</sub> is also highly desirable.

We are very grateful to Dr. S. Gama for supplying some of the raw materials, to Dr. I. Torriani for the X-ray diffractogram, and to D. Silva (IG-Unicamp) for the SEM and microprobe analysis. This work is supported by the Brazilian science agencies FAPESP (Fundação de Amparo a Pesquisa do Estado de São Paulo) and CNPq (Conselho Nacional de Desenvolvimento Científico e Tecnológico).

<sup>1</sup> J. Akimitsu, Symposium on Transition Metal Oxides, Sendai, January 10, 2001; J. Nagamatsu et al., Nature **410**, 63 (2001).

<sup>2</sup> S. L. Bud'ko et al., Phys. Rev. Lett. **86**, 1877 (2001).

<sup>3</sup> G. Karapetrov et al., cond-mat/0102312.

<sup>4</sup> J. Kortus et al., cond-mat/0101446.

<sup>5</sup> N. I. Medvedeva et al., cond-mat/0103157.

<sup>6</sup> D. C. Larbalestier et al., cond-mat/0102216.

<sup>7</sup> W. N. Kang et al., cond-mat/0103161.

<sup>8</sup> Y. Wang et al., cond-mat/0103181.

<sup>9</sup> P. C. Canfield et al., cond-mat/0102289.

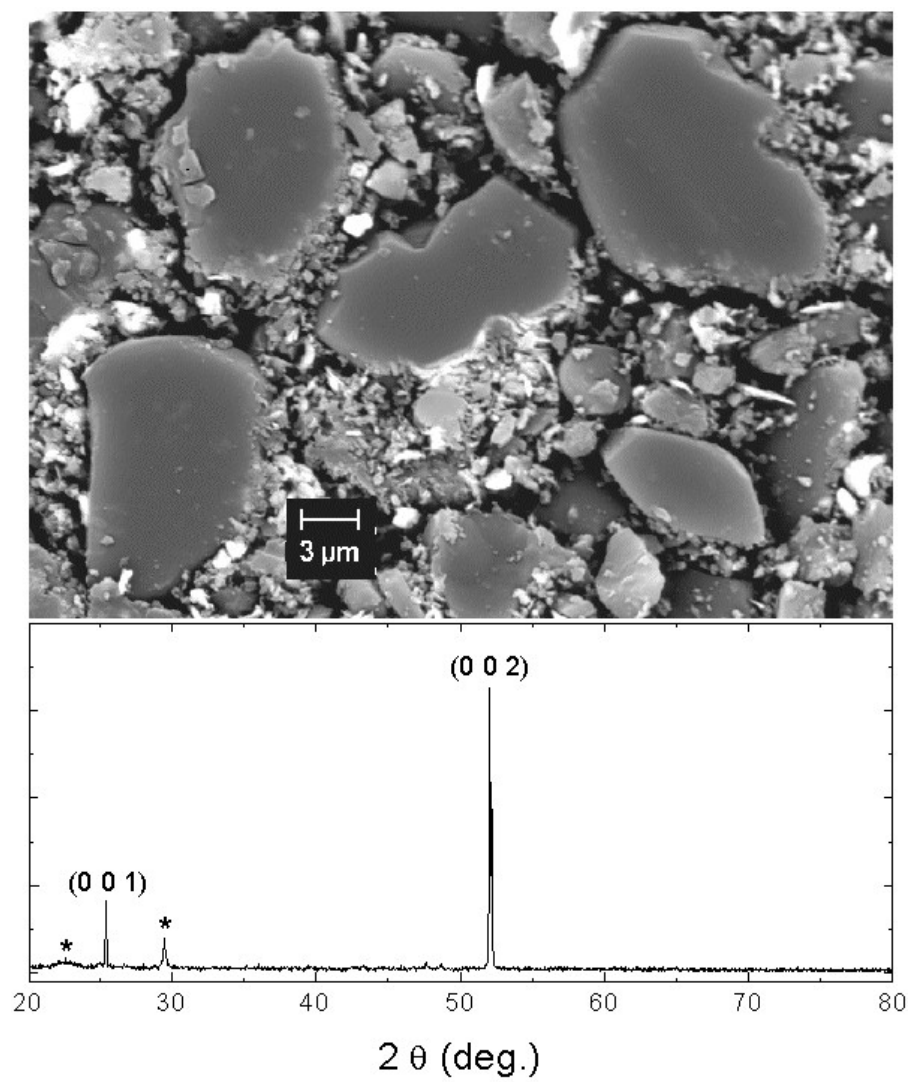
- <sup>10</sup> D. K. Finnemore et al., cond-mat/0102114.
- <sup>11</sup> K. -H. Müller et al., cond-mat/0102517.
- <sup>12</sup> M. Tinkham, *Introduction to Superconductivity* (McGraw-Hill, New York, 1996).
- <sup>13</sup> G. Blatter et al., Rev. Mod. Phys. **66**, 1125 (1994).
- <sup>14</sup> H. H. Wen et al., cond-mat/0102436.
- <sup>15</sup> C. P. Bean, Rev. Mod. Phys. **36**, 31 (1964).
- <sup>16</sup> D. Saint-James and P. G. de Gennes, Phys. Letters **7**, 306 (1963).
- <sup>17</sup> D. Saint-James, G. Sarma and E. J. Thomas, *Type II Superconductivity* (Pergamon, 1969).

FIG. 1. Top: SEM picture showing the well aligned crystallites and inter-crystallite material. Bottom: X-ray diffraction pattern showing only the (001) and (002) peaks of  $\text{MgB}_2$ , plus two spurious peaks indexed as  $\text{SiO}_2$ .

FIG. 2. Upper critical field  $H_{c2}$  vs. Temperature phase diagram, for both sample orientations. The stars represent the  $H_{c2}$  vs. T line from Ref. 11. The inset shows the real component  $\chi'$  of the ac susceptibility vs. temperature, measured at several dc fields for both orientations. Open symbols are for the  $H//ab$  curves and solid symbols for  $H//c$ .

FIG. 3. Magnetization loops at 5 K for both sample orientations, showing a superconducting hysteresis on a ferromagnetic background. The inset shows a dc magnetization vs. temperature curve at 10 Oe, showing a sharp transition at 39.2 K and a 67% recovery of diamagnetism for the FCC curve.

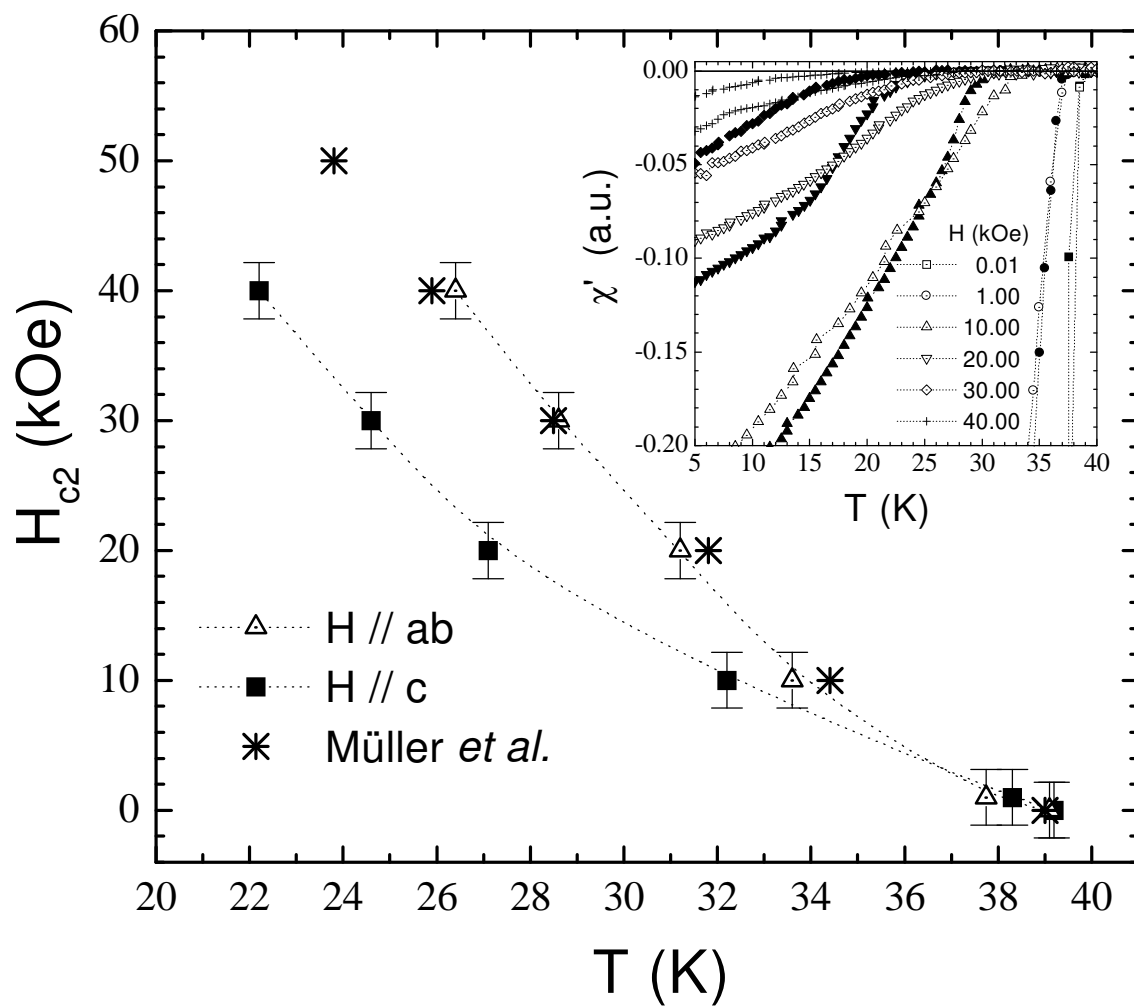
FIG. 4. Magnetization loops ( $M$  vs.  $H$ ) at 45 K (above  $T_c$ ) for both sample orientations, showing the ferromagnetic behavior of our sample. The inset shows the hysteretic behavior at low fields.



de Lima *et al.*

FIG. 1

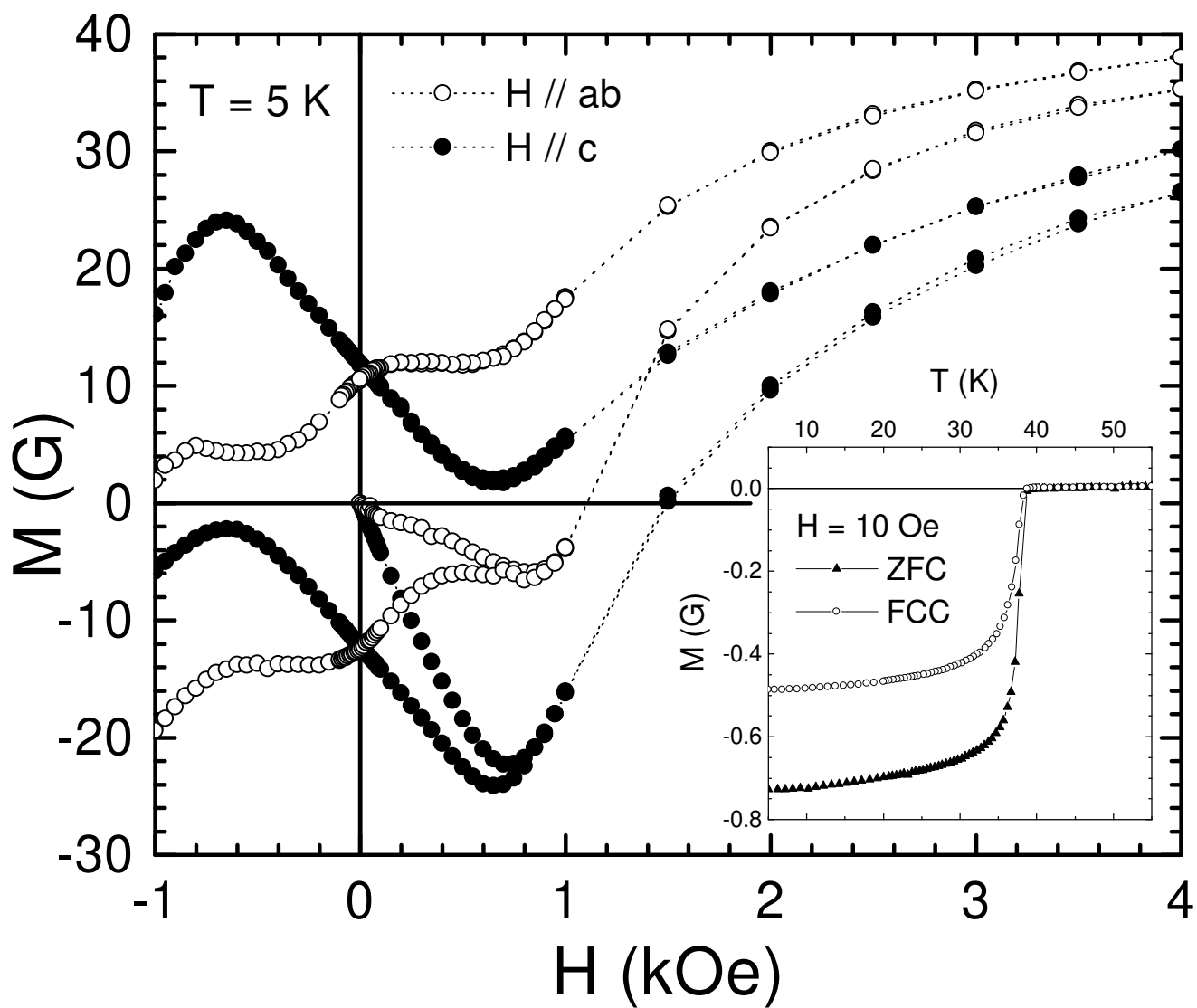




de Lima *et al.*

Fig. 2



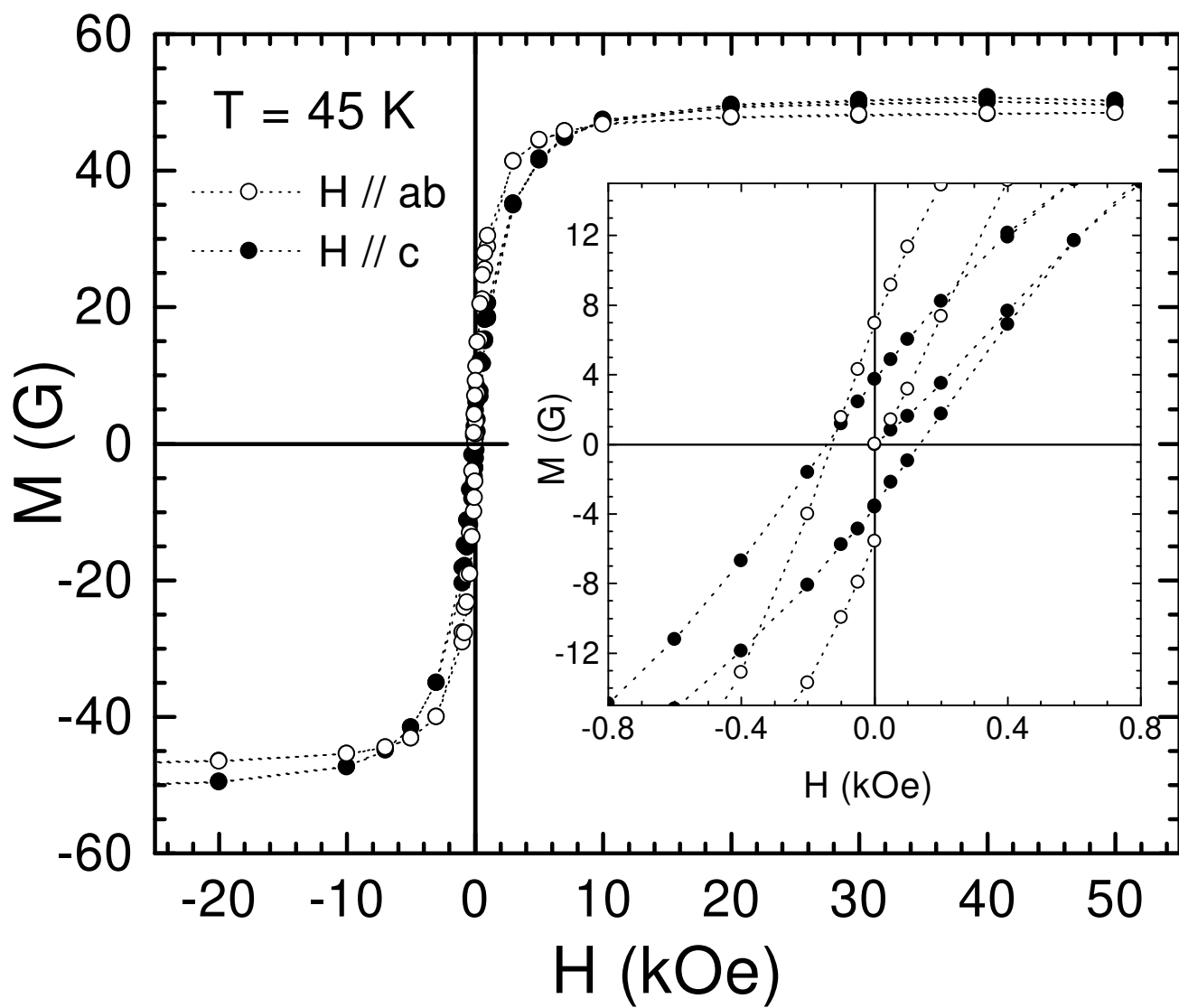


de Lima *et al.*

FIG. 3







de Lima *et al.*

FIG. 4

